An advanced spectrum analysis of radio-wave signals using non-collinear anomalous light scattering

Technical Report No. 647

Principal contributors:

Alexandre S. Shcherbakov and Adán Omar Arellanes.

National Institute for Astrophysics, Optics, and Electronics (INAOE), Puebla, Mexico.

National Institute for Astrophysics, Optics, and Electronics (INAOE),

Puebla, Mexico.

Department for Optics, INAOE

Index

ABSTRACT

We present principally new acousto-optical cell providing an advanced wide-band spectrum analysis of ultra-high frequency radio-wave signals. For the first time we apply recently developed approach with the tilt angle to a one-phonon non-collinear anomalous light scattering. In contrast to earlier cases, now one can exploit a regime with the fixed optical wavelength for processing a great number of acoustic frequencies simultaneously in the linear regime. The chosen for cell rutile-crystal combines a moderate acoustic velocity with low acoustic attenuation and allows us a wide-band data processing within GHz-frequency acoustic waves. We have created and experimentally tested a 6 cm aperture rutile-made acousto-optical cell providing the central frequency 2.0 GHz, frequency bandwidth ~ 0.52 GHz with the frequency resolution about 68.3 kHz and ~ 7620 resolvable spots. Similar cell permits designing an advanced ultra-high-frequency arm within recently developed multi-band radio-wave acousto-optical spectrometer for astrophysical studies. This spectrometer is intended to operate with a few parallel optical arms for processing the multi-frequency data flows within astrophysical observations. Keeping all the instrument's advantages of previous schematic arrangement, now one can create the highest-frequency arm using the developed rutile-based acousto-optical cell. It permits optimizing the performances inherent in that arm via regulation of both the central frequency and the frequency bandwidth for spectrum analysis.

Keywords: Spectrometers and spectroscopic instrumentation, Acousto-optical materials, Dynamic diffraction grating, Acousto-optical devices, Spectroscopy, high resolution.

1. INTRODUCTION

Recently [1], a pioneer approach to designing the acousto-optical (AO) spectrometer for radio-astronomy had been schematically proposed by our group as well as analyzed using both the practical estimations and some preliminary proof-of-principal experiments. The novelty of that proposal was in principally higher parallelism in a wideband analogue signal processing with various frequency performances simultaneously. Radio-wave signals give birth to a large amount of dynamic diffraction acoustic gratings in AO cells. Each grating is conditioned by a frequency harmonic of the incoming radio-wave signal that deflects the preliminary expanded incident monochromatic optical beam. This is why each incident optical beam is converted into a large amount of individual light beams creating individual parallel frequency channels for the corresponding radio-wave signal processing. As a result, the intensities of individual light beams are governed by the amplitudes and phases of frequency harmonics from the incoming radio-wave signals. Then, all the individual light beams are focused by the Fourier-integrating lenses on a CCD photo-detector for the subsequent joint high-bit-rate electronic processing. At this point one yields at the united versatile instrument, which provides comprehensive investigations of astrophysical objects simultaneously with precise synchronization in various frequency scales. At that moment, we had restricted ourselves by only three similar spatial optical arms for data processing, see Fig. 1.

Each individual spatial arm exhibits its own original performances to provide parallel multi-band observations of astrophysical objects within a few different scales at the same time. Therefore, one can exploit different materials for AO cells operating within various regimes in different frequency ranges. The first (low-frequency, TeO_2-cell) and second (middle-frequency, bastron cell) spatial arms had been described early [1,2], so that they need not additional comments. Now our attention is focused on the third, highest frequency arm of processing based on a rutile cell, which is intended for direct spectrum analysis of UHF radio-wave signals with the central frequencies about 2.0 GHz and the frequency bandwidth ~ 500 MHz. In so doing, we consider the specially designed wide-aperture UHF AO cell based on the rutile single crystal as an appropriate key opto-electronic device representing the corresponding dynamic grating.

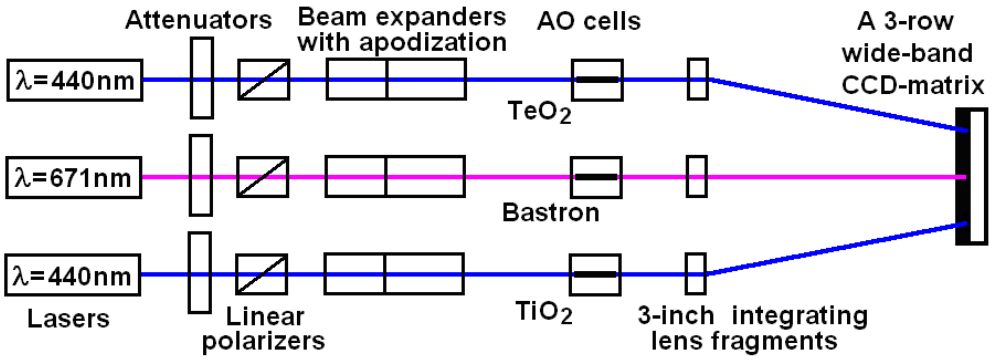

Fig. 1. The proposed schematic arrangement of the spatial arms in the AO spectrometer. The lower arm is related to the rutile AO cell under analysis.

1.1. Frequency characterization for two low-loss uniaxial crystals

At the moment, only two low-loss crystals, providing the slow-shear elastic modes exploitation, can be considered for realizing a one-phonon non-collinear anomalous light scattering due to their more or less acceptable physical characteristics. These crystals exhibit moderate linear acoustic losses, low enough velocities of acoustic waves, and are able for a reasonable efficiency for anomalous light scattering. Let's consider them sequentially under the condition that the total losses per the optical aperture D = 6 cm should be about $\tilde{B} \approx 8$ dB/ap.

1.1.1. Lithium niobate: $LiNbO_3$. S[100] 35° Y.

For slow-shear mode S[100] 35° Y in $LiNbO_3$-crystal with $V = 3.6 \times 10^5$ cm/s and $\Gamma \approx 0.28$ dB/(cm GHz^2), such a requirement leads to the acoustic frequency $f_C = [\tilde{B}/(D\,\Gamma)]^{1/2} \approx 2.196$ GHz. Then, this crystal has quite moderate birefringence, for example, $N_O \approx 2.4317$, $N_E \approx 2.3257$ at $\lambda = 440$ nm [3]. By this it means that the maximal central frequency for a one-phonon light scattering is limited by about $f_C \approx V\,\lambda^{-1}\,|N_E^2 - N_O^2|^{1/2} \leq 5.8$ GHz. After that, one can estimate the expected resolution within the one-phonon light scattering. The frequency resolution is $\delta f_T = V/D \approx 60.0$ kHz at the light intensity level of 0.405 (the Rayleigh criterion). Unfortunately, this crystal exhibits strong photorefraction in blue and ultraviolet range. Of course, $LiNbO_3$ crystal has the opportunity to shift the optical absorption edge to the ultraviolet light by being doped with Mg [4]. The previous would enable the use of such crystal for 370 nm optical wavelength and also that doping would reduce the optical absorption by almost four times. The presence of a dopant leads to the possibility of exploiting $LiNbO_3$-crystal at even $\lambda = 370$ nm, but only under action of very low-intensity optical beams, which cannot be realized in radio-wave AO spectrometers.

1.1.2. Rutile TiO_2:S[110] $[1\bar{1}0]$.

In 2008, a rutile-crystal based Bragg AO cell with 3 GHz bandwidth had been reported in connection with the development of ultra-wide band AO spectrometer for astrophysical applications [5]. This cell had been designed for operation at $\lambda = 488$ nm, and its response was centered at ~ 5 GHz with the flatness better than ~ 3 dB. However, the optical aperture was small (1.65 cm), so that frequency resolution was low (200 kHz). These theoretical data for the spectral resolution cannot be considered directly in the presence of high acoustic losses about of 11 dB per aperture for AO cell, because the effect of nonlinear apodization [6] must be additionally estimated. Let us consider an opportunity to exploit almost this geometry of AO interaction for realizing a one-phonon light scattering. Broadly speaking, due to its spectral range is $\Delta\lambda \approx 0.45$-$6.0$ μm, the main refractive indices of a TiO_2-crystal are about $N_O \approx 2.853$ and $N_E \approx 3.216$ at $\lambda \approx 440$ nm, one can expect the maximal central frequency for a one-phonon light scattering [7] close to $f_C \approx V\,\lambda^{-1}\,|N_E^2 - N_O^2|^{1/2} \approx 10$ GHz. Then, for the chosen level $\tilde{B} = 8.1$ dB/ap one yields at $f_C = [\tilde{B}/(D\,\Gamma)]^{1/2} \approx 2.0$ GHz with $\Gamma = 0.337$ dB/(cm GHz^2) due to linear acoustic losses equals to 1.348 dB/cm. Reasoning from $V = 3.3 \times 10^5$ cm/s for the slow-shear mode

S[110] [$1\bar{1}0$] in rutile, one can estimate that theoretical frequency resolution of AO cell in conventional scheme of spectrum analyzer [8] will be $\delta f_T = V/D \approx 55$ kHz.

In our opinion, these estimations are looking more attractive for the rutile crystal in spite of possible effect from worsening practical factors. Therefore, the rutile-based AO cell can be selected as the best choice.

2. USAGE OF THE TILT-ANGLE BASED APPROACH TO THE ONE PHONON ANOMALOUS LIGHT SCATTERING IN RUTILE

Now, we are going to apply the recently developed for the two-phonon light scattering approach with the tilt angle [9], to the one-phonon non-collinear anomalous AO interaction. This is why in contrast to the earlier case, now one can exploit the regime with the fixed optical wavelength for processing a large amount of various acoustic frequencies in linear regime. Such an advanced approach represents the light scattering in terms of two surfaces for the refractive indices of ordinary (see the internal dark sphere) and extraordinary (see the external faint ellipsoid) light waves for a tetragonal rutile crystal at the fixed optical wavelength λ at $N_E \geq N_O$, see Fig. 2. The chosen rutile crystal combines a moderate acoustic velocity and relatively low acoustic attenuation allowing the operation over UHF acoustic waves. The sizes of both the sphere and the ellipsoid will be varied depending on λ due to remarkable optical dispersion of the rutile crystal within the visible range.

The vertical axis in Fig. 2 is oriented along the optical axis [001] of rutile crystal, while orientation for a pair of the horizontal axes depends on the chosen elastic modes. In rutile, we have taken them as $[110]$ and $[1\bar{1}0]$ axes for the slow-shear acoustic mode. This figure represents the vector diagram, illustrating an opportunity for the one-phonon non-collinear anomalous light scattering through various angles; which includes an optimal acoustic frequency with the refractive indices adequate to the chosen λ. A pair of vectors, going from the coordinate origin, i.e. from geometric center of surfaces, represents the optical wave vectors describing the corresponding orders of light scattering, whereas an acoustic wave vector $\vec{K}$ reflects the anomalous scattering process. The tilt angle ϕ characterizes an angle between the optical axis and the geometrical plane for scattering, which includes all the optical and acoustic wave vectors. The availability of the angle ϕ reflects the existence of an additional physical degree of freedom inherent in the one-phonon anomalous light scattering. This degree of freedom permits the fixed optical wavelength to exert control over various acoustic frequencies scattered through different angles.

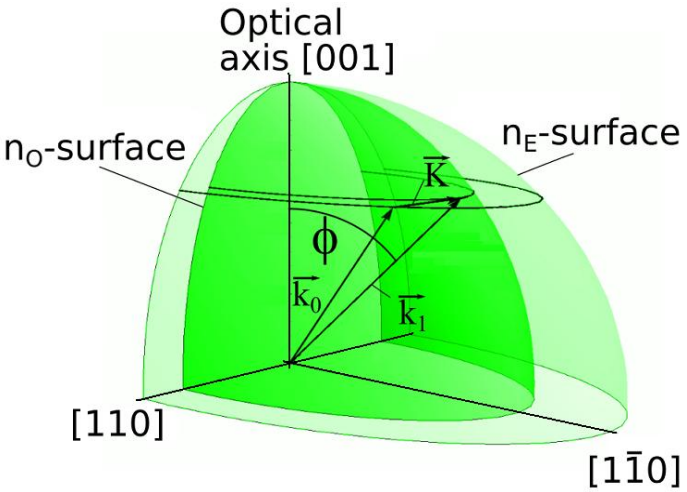

Fig. 2. The vector diagram for the one-phonon anomalous light scattering in rutile, where ϕ is the tilt angle.

Rutile is a uniaxial crystal, so that $n_O \equiv N_O$ is the main refractive index for the ordinary state of polarization whose 3D-representation is a sphere. The refractive index n_E for the extraordinary polarization ($n_E > n_O$) depends on a direction of light propagation in a crystal, and its 3D-representation has the form of an ellipsoid. We are interested in tilts from the [001]-axis, therefore, one can consider the angle $\phi \in [0, \pi/2]$ of a tilt from the [001] -axis. Considering the geometry, one can obtain

$$\tan\phi = \lambda\, f_C\, (N_E / N_O) \cdot [V^2 (\, N_E^2 - N_O^2\,) - \lambda^2\; f_C^2\,]^{-1/2}, \tag{1}$$

were [10]

$$N_O = \left[\, 5.913 + \frac{2.441 \times 10^7}{-8.03 \times 10^6 + 100 \cdot \lambda^2}\, \right]^{1/2},$$

$$N_E = \left[\, 7.197 + \frac{3.322 \times 10^7}{-8.43 \times 10^6 + 100 \cdot \lambda^2}\, \right]^{1/2}, \tag{2}$$

due to optical dispersion; the wavelength λ should be taken in nanometers in Eq. (2).

Now, keeping in mind the requirements of the best achievable frequency performances, the detailed analysis can be proceeded from the optical aperture D of the AO cell, restricted by an available sample of the chosen crystal with a given factor Γ of acoustic attenuation. Taking a permissible value $\tilde{B}$ dB/aperture of acoustic losses, one can find the central frequency for a one-phonon non-collinear anomalous light scattering as $f_C = [\, \tilde{B} /(\Gamma\ D)]^{1/2}$. Then, the chosen rutile crystal gives the acoustic velocity $V = 3.3 \times 10^5$ cm/s and the factor $\Gamma = 0.337$ dB/cm·GHz^2 [11] as well as the main refractive indices $N_E = 3.1994$ and $N_O = 2.8403$ at $\lambda = 440$ nm. These indices should be substituted in Eq. (1) to explain the tilt angle ϕ mentioned above at the central frequency f_C. Using these details, one can estimate the theoretical performances of the rutile-made AO cell.

3. THEORETICAL PERFORMANCES OF THE RUTILE-BASED AO CELL FOR DIRECT ANALYSIS OF UHF RADIO-WAVE SIGNALS

To provide direct spectrum analysis of UHF radio-wave signals the rutile-based AO cell operating in the regime of one-phonon non-collinear anomalous light scattering with so-called "optimal phase-matching" can be chosen. As it had been shown [12], due to taking similar modified geometry of AO interaction, exactly two acoustic wave vectors will intersect the internal optical surface of refractive indices. Therefore, the precise Bragg matching can be fulfilled at a pair of different acoustic frequencies. As a result, close to perfectly symmetric profile of the frequency band-shape will be potentially formed. Therefore, two maxima of a new band-shape will be situated at frequencies almost equidistant from the central tangentially matching frequency. In this case, both the central frequency f_C and the frequency bandwidth Δf_A the for one-phonon anomalous light scattering are given by [12]

$$\text{a)}\ \ f_C = \frac{V}{\lambda}\sqrt{|\, n_E^2 - n_O^2\,|}\,,$$
$$\text{b)}\ \ \Delta f_A \approx 2V\sqrt{2n_E/(\lambda L)}\,, \qquad (3)$$

where n_E is the refractive index of incident light and L is the initial length of AO interaction. Expression for Δf_A in Eq. (3b) does not include the frequency f_C in the contrast with the corresponding formula for the normal light scattering $\Delta f_N \sim 1/ f_C$ [13,14], leading to fast decreasing Δf_N when f_C grows. The sub-indices in the frequency bandwidth $\Delta f_{A,N}$ stand for the anomalous and the normal light scattering, respectively. The ratio n_E / λ in Eq. (3b) can be considered as a physical degree of freedom to increase the frequency bandwidth Δf_A, as it is seen from Eq. (3b), in such a way that the central frequency f_C will be fixed. The corresponding plot for the visible range is presented in Fig. 3. Thus the widest frequency bandwidth Δf_A with the fixed central frequency f_C can be reached at blue light about of $\lambda = 440$ nm.

In a rutile crystal, one can choose the process using the elastic mode S[110][$1\bar{1}0$], so that $V = 3.3 \times 10^5$ cm/s, $n_E \approx 2.8528$ at $\lambda = 440$ nm and L = 0.2 cm. Using Eqs. (3b), one can estimate theoretically $\Delta f_A \geq 530$ MHz and $f_C \approx 2.0$ GHz, while $\Delta f_N \approx 35.3$ MHz at the same central frequency f_C and other parameters. The use of Eq. (1) and these parameters give the tilt angle $\phi = 11.72°$. For the taken set of material parameters, estimating the Klein-Cook parameter at the minimal frequency of the bandwidth Δf_A, i.e. at $f_{min} = f_C - (\Delta f_A/2) = 1735$ MHz gives $Q = (2\pi / n_E)\cdot(\lambda L\, f_{min}^2 / V^2) > 5.35 \times 10^2$, which strongly provides the Bragg regime of scattering at f_{min}. The obtained data mean that $\Delta f_A / f_C \approx 26.5\%$, which can be improved, evidently, only through exploiting much more complicated and expansive phased-array technique for arranging the piezoelectric transducer [12].

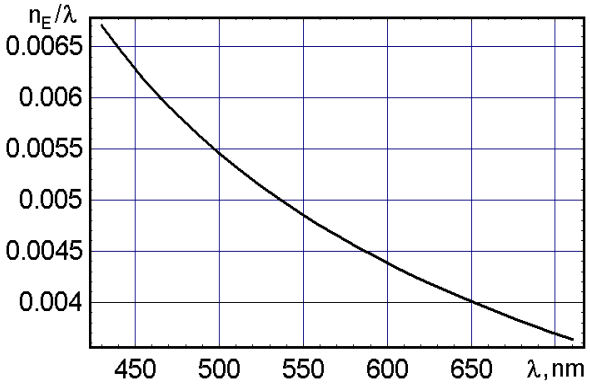

Fig. 3. The ratio n_E / λ versus the optical wavelength λ at the fixed $f_C \approx 2.0$ GHz in rutile single crystal.

The number N of resolvable spots is limited by a few independent conditions, which can be expressed as follows. In so doing, one can use the expression

$$N_1 \le (\delta f)^{-1} \cdot \Delta f_A = \frac{D}{V} \cdot \Delta f_A \approx 2D \sqrt{\frac{2n_E}{\lambda L}}, \tag{4}$$

which does not depend on the central frequency. Then, keeping in mind an available for us aperture of the rutile crystal, one can take a little bit unexpected value $\tilde{B}$ = 8.1 dB/aperture as an acceptable level of acoustic losses along the AO cell's aperture and find an allowable aperture D

$$D \le \tilde{B} \Gamma^{-1} f_C^{-2} \approx 6\, cm, \tag{5}$$

due to $\Gamma \approx 0.337$ dB / (cm·GHz^2). However, one has to note that the information related to the attenuation level for this acoustic mode is rather contradictory, so that the taken value of Γ ought to be considered as a reference one. Substituting Eq.(5) into Eq.(4), one can find

$$N_2 \le \frac{\tilde{B}}{\Gamma V f_C^2} \cdot \Delta f_A \approx 9{,}650\,. \tag{6}$$

By this it means that in the case of D ≈ 6.0 cm at f_C = 2.0 GHz, one can expect theoretically about $N_T \approx 9650$ resolvable spots with the TiO_2-cell under consideration, while the corresponding frequency resolution $\delta f_T = V / D \approx 55$ KHz.

The efficiency of anomalous AO interaction in a crystal can be characterized by the modified AO figure of merit $M_2 = n_O^3 n_E^3 p_{eff}^2 / (\rho V^3)$, where n_O and n_E are the corresponding refractive indices, ρ is the material density of a rutile crystal, and p_{eff} is the corresponding effective photo-elastic constant. To determine the magnitudes of both p_{eff} and M_2 one can apply the recently developed approach [9] to the case of the pure slow-shear elastic mode $S[110][1\bar{1}0]$ in a TiO_2 -crystal.

To obtain the AO figure of merit M_2 inherent in the selected cut of a TiO_2 crystal, first, the effective photo-elastic constant p_{eff} has to be found. The TiO_2 single crystal belongs to the 4/mmm–tetragonal symmetry group and it allows existing pure shear elastic waves with the wave vector $\vec{K} \parallel [110]$ and the displacement vector $\vec{u} \parallel [1\bar{1}0]$, see Fig. 4.

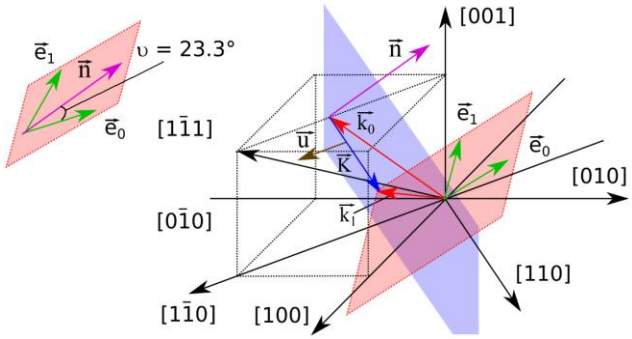

Fig. 4. Vector diagram for a one-phonon non-collinear anomalous light scattering in the rutile-based AO cell.

Each dynamic acoustic grating can be characterized by its deformation tensor of the second rank. Due to $\vec{q} = \vec{K}/|\vec{K}| = (1/\sqrt{2})(1,1,0)$ and $\vec{u} = (1/\sqrt{2})(1,-1,0)$, so that the corresponding deformation tensor can be converted into a 6-dimension vector $\bar{\gamma} = 0.5 \cdot (1,-1,0,0,0,0)$ [5]. Then, one arrives at the product $p\bar{\gamma} = 0.5(p_{11} - p_{12}) \cdot (1,-1,0,0,0,0)$ with $p_{11} = 0.011$ and $p_{12} = 0.172$ [11], and at $p_{eff} = \vec{e}_1 (p\gamma) \vec{e}_0$, where the vectors $\vec{e}_0$ and $\vec{e}_1$ describe the polarization states of incident and scattered light beams, respectively. Within the non-collinear interaction, the eigen-vectors of polarization $\vec{e}_0$ and $\vec{e}_1$ of the incident and scattered light beams, respectively, for the wave vector of the incident light $\vec{k}_0 = (-(1/\sqrt{2})\sin\phi, (1/\sqrt{2})\sin\phi, \cos\phi)$, are equal to

$$\vec{e}_0 = ((1/\sqrt{2})[-\cos\upsilon \cdot \cos\phi + \sin\upsilon],\ (1/\sqrt{2})[\cos\upsilon \cdot \cos\phi + \sin\upsilon],\ \cos\upsilon \cdot \sin\phi), \quad (7)$$

$$\vec{e}_1 = ((1/\sqrt{2})[-\cos\upsilon + \cos\phi \cdot \sin\upsilon],\ (1/\sqrt{2})[-\cos\upsilon\cos\phi \cdot \sin\upsilon],\ -\sin\upsilon \cdot \sin\phi). \quad (8)$$

Here, the angle υ is depicted in Fig. 4. These eigen-vectors lead to the following result

$$p_{eff} = \vec{e}_1 (p\gamma) \vec{e}_0 = 0.5(p_{11} - p_{12}) \cdot [\cos(2\upsilon) \cdot \cos\phi]. \quad (9)$$

With $\upsilon \approx 23.3^o$ [5] and $\phi \approx 11.72^o$ one yields $p_{eff} \approx 0.0542$. Using $n_O = 2.8403$ and $n_E = 2.8528$ at λ = 440 nm with $\rho \approx 4.23\ g/cm^3$ and $V \approx 3.3 \times 10^5\ cm/s$ [15], one can obtain

$$M_2 = n_O^3 n_E^3\ p_{eff}^2 / (\rho V^3) \approx 9.355 \cdot 10^{-18}\ s^3/g, \quad (10)$$

which looks rather acceptable.

4. PRE - EXPERIMENTAL CONSIDERATION

4.1. An opportunity of regulating the Gaussian apodization

Now, the apodization of the incident light beam within the AO spectrum analyzer can be considered. Let us place the origin of the coordinate x along acoustic beam so that the point $x = 0$ will be associated with the middle of the optical aperture D of an AO cell playing the role of an equivalent diaphragm. One can suppose that the electric field amplitude profile $A(x)$, inherent in the issuing beam of a laser and reaching an AO cell's aperture, is usually rather close to the Gaussian shape [16], so that one can write (in both physical and dimensionless variables) that

$$\begin{aligned} &\text{a)}\ A(x) = A_0 \exp[-\xi x^2] = A_0 \exp[-\beta y^2], \\ &\text{b)}\ I(y) = |A_0|^2 \exp[-2\beta y^2]. \end{aligned} \tag{11}$$

Here, $y = x/D$ is the normalized dimensionless coordinate along the optical aperture D of a crystal, so that $y \in \{0,1\}$, while ξ and $\beta = \xi D^2$ are physical and dimensionless apodization profile parameters for the Gaussian function.

The key point of this section is based on the statement: a multi-prism beam expander can be exploited for matching the initial size of laser light beam with the optical aperture of a large-aperture AO cell in the plane of light scattering, i.e. to provide a one-dimensional expanding of the laser beam together with its Gaussian apodization. For this purpose initially one has to describe briefly a multi-prism beam expander in minimally needed details and to characterize the issuing laser beam of a laser.

It is well known that a multi-prism beam expander can be designed relatively simply and compact using right-angle prisms. With the standard formula for the light refraction [2] by the first facet, i.e. by the border air/glass $\sin\varphi = n \sin\delta$, where n is the refractive index of a glass, one can obtain the factor of beam expanding

$$\begin{aligned} &\text{a)}\ B_1 = \frac{d_1}{d_0} = \frac{\sqrt{(n^2 - \sin^2\varphi)[1 - n^2 \sin^2(\alpha - \delta)]}}{n \cos\varphi \cos(\alpha - \delta)}, \\ &\text{b)}\ \delta = \arcsin\left(\frac{\sin\varphi}{n}\right), \end{aligned} \tag{12}$$

where α is the top angle of the prism. In the simplest case, when all the glass prisms are identical to one another and the angles φ of incidence are the same for all of them, one can write $B_m = (B_1)^m$ and obtain the needed expanding, where m is the parameter of expanding. Involving, in particular, even number of the Littrow prisms (i.e. the right-angle prisms 30° - 60° - 90°), the beam direction can be saved with an accuracy of some spatial parallel shift. Equation (12) shows that initially in-phase beam with a Gaussian intensity profile, whose full width can be estimated at a given level (for instance, at a level of e^{-2}), will be expanded

by a suitable prism in the same proportion $B_m = d_m / d_0$ on the given intensity level as well due to using an approximation of the geometrical optics, see Fig. 5. Then, Eq.(12) determines practically important dependence of B_m and d_m on the angle φ of light incidence on the input facet of a beam expander. The analysis shows that the case of a 4-prism glass expander with n = 1.5 and $\alpha = 30°$ is perfectly acceptable for our needs.

Then, one has to characterize the issuing laser beam of a laser. In so doing, let us select beam parameters of the above-chosen laser CL442-050-S (CrystaLaser) with the option 0.7 mm beam diameter at a level of $e^{-2} \approx 0.1353$ and 1.0 mrad beam divergence. The corresponding plot for the light intensity distribution is depicted in Fig. 6.

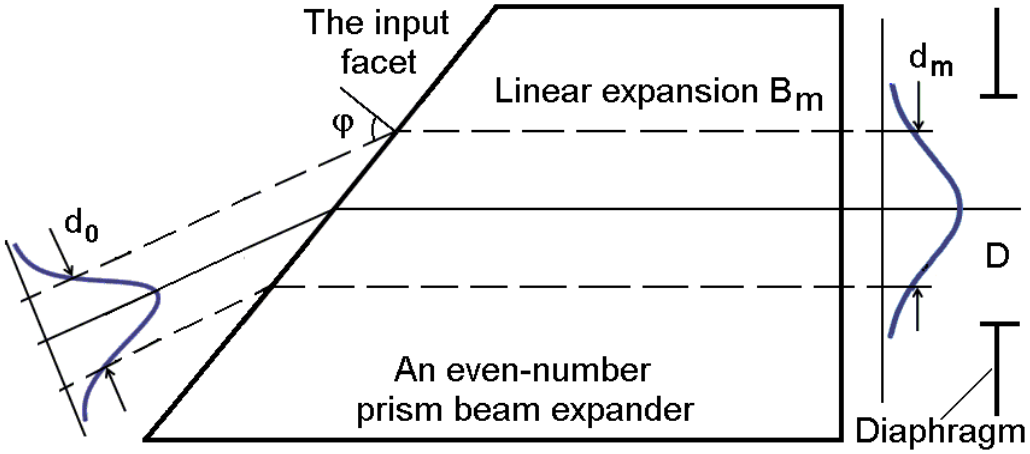

Fig. 5. A Gaussian profile passing through an even-number prism beam expander with an equivalent diaphragm D.

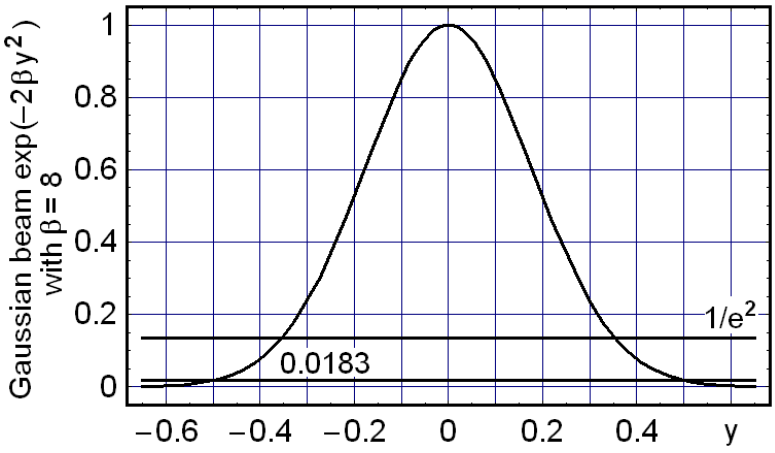

Fig. 6. Levels of estimations for a Gaussian beam.

Taking the window $y \in [-0.5, 0.5]$ in Fig. 6, i.e. $D = 1\,mm$ in dimensional units, one yields the formal equality $[x, mm] = y$. The beam diameter 0.7 mm is now associated with full width 0.7 and corresponds to the level e^{-2}. Analyzing Fig. 6, one can find practical identity of this distribution with the spatial dependence $\exp(-2\beta y^2)$ with $\beta = 8$, which

exhibits the intensity level $I_{\beta=8} \approx 0.0183$ at $y = \pm 0.5$. By this it means that the chosen light intensity distribution can be considered as a basic one with the maximal apodization parameter $\beta_{max} = 8$ for the further manipulations related to expanding this beam on wider aperture with smaller values of β. Here, the aperture $60\,mm$ will be mainly considered, that corresponds to the above-formulated needs. In particular, to realize Gaussian apodization with $\beta = 8$ for a $60\,mm$-aperture, one can exploit the above-chosen output dark-blue laser beam with $d_0 = 1\,mm$ (at the intensity level $I_{\beta=8} \approx 0.0183$) and simply expand it by 60 times. However, if the apodization parameter should be smaller than $\beta = 8$ for that a $60\,mm$-aperture, a few additional manipulations have to be done. For this purpose, first one has to determine the intensity levels I_β for the desirable values of β. Using Fig. 7, one can find for $\beta \le \beta_{max}$ that, for instance: $I_{\beta=2} \approx 0.36788$, $I_{\beta=3} \approx 0.2231$, $I_{\beta=4} \approx 0.1353$, and $I_{\beta=6} \approx 0.04979$ related to $y = \pm 0.5$. Then, these levels should be applied to the profile with $\beta = 8$, see Fig. 7, to find the corresponding values $y_m = 0.25\sqrt{-\ln I_m}$, which are $y_2 \approx 0.2500$, $y_3 \approx 0.3062$, $y_4 \approx 0.3536$, and $y_6 \approx 0.4330$.

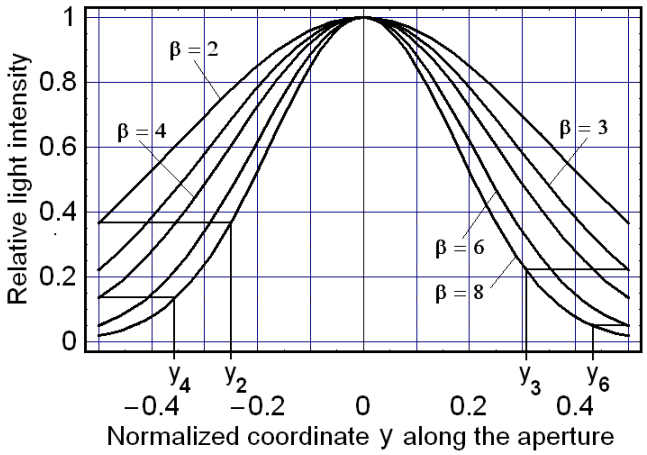

Fig. 7. The role of the apodization factor β.

The needed expansion factors are equal to $B_m = 60/(2y_m)$, i.e. $B_2 \approx 120$, $B_3 \approx 98.0$, $B_4 \approx 84.8$, $B_6 \approx 69.3$, and $B_8 = 60$ for the corresponding β_m. Each of these values requires the corresponding angle φ_m of light incidence on the prisms, see Fig. 8, i.e. $\varphi_2 \approx 77.03^0$, $\varphi_3 \approx 76.31^0$, $\varphi_4 \approx 75.76^0$, $\varphi_6 \approx 74.98^0$, and $\varphi_8 = 74.33^0$, which provide the relative optical transmission factors T_m i.e.: $T_2 \approx 0.45$, $T_3 \approx 0.50$, $T_4 \approx 0.52$, $T_6 \approx 0.55$, and $T_8 = 0.58$.

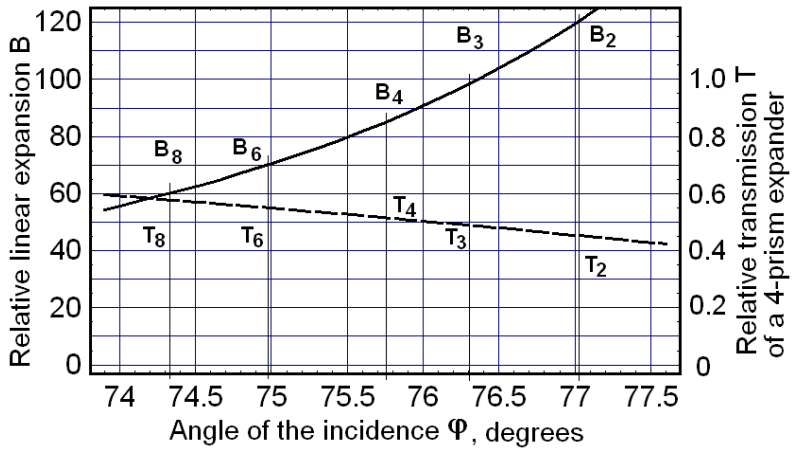

Fig. 8. Linear expansion B (solid line) and transmission T (dashed line) vs. the angle φ of light incidence for a 4 prism beam expander made of the Littrow prisms with $n = 1.5$ and $\alpha = 30^0$.

Finally, one can determine total efficiencies ν_m of similar expanding. In so doing, one has to calculate them as

$$\nu_m = T_m \cdot \frac{\int_{-y_m}^{y_m} Exp[-2 \cdot 8 \cdot y_1^2]\, d\, y_1}{\int_{-0.5}^{0.5} Exp[-2 \cdot m \cdot y_2^2]\, d\, y_2}\,, \tag{13}$$

where both the transmission factors T_m of a 4-prism expander, operating with the optimal angular orientation of each prism, by itself and contributions of the developed procedure specific to the expanded Gaussian apodization are taken into account. Due to Eq. (13) gives the following values $\nu_2 \approx 0.225$, $\nu_3 \approx 0.306$, $\nu_4 \approx 0.368$, $\nu_6 \approx 0.476$, and $\nu_8 = T_8 = 0.58$, one can plot a set of theoretical light intensity distributions $I_{Em} = \nu_m \exp[-2 m y^2]$ for the expected Gaussian apodization profiles at the output facet of a 4-prism beam expander, see Fig. 9a. The corresponding experimental plots for the case of 4-prisms with $n = 1.5$ and $\alpha = 30^0$ are presented in Fig. 9b.

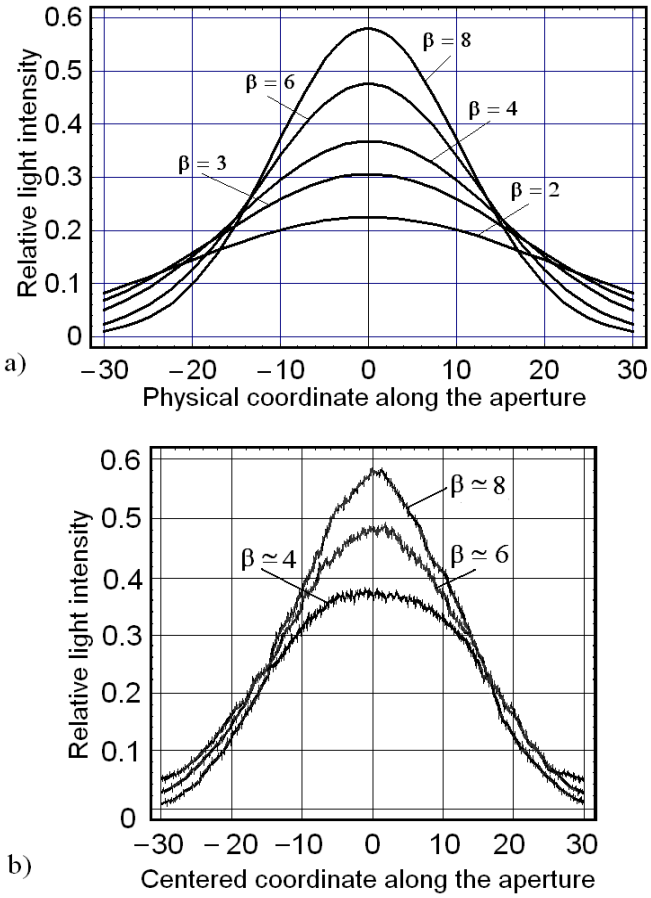

Fig. 9. Profiles I_{Em} at the output facet of a 4-prism beam expander: a) theoretical plots, b) experimental traces.

4.2. Rutile AO cell

The above-described AO cell can potentially work in specifically elaborated regime [1,2] at optical wavelength $\lambda \approx 440$ nm, which combines the convenience of operating in the visible range with good enough transparency of this material with blue light, from the single frequency solid-state laser CL-442-050-S (CrystaLaser). The rutile-based AO cell of 6 cm aperture is theoretically able to manage the UHF radio-wave signals whose good enough performances can be estimated at the central frequency about of 2.0 GHz by the frequency bandwidth about 530 MHz and theoretical frequency resolution $\delta f_T \approx 55$ KHz providing theoretically $N_T \approx 9.65 \cdot 10^3$ of resolvable spots. In the scheme of standard AO spectrum analysis (see Fig. 10), this number N means in fact the number of parallel frequency channels for spectral data processing. The beam shaper included a variable optical attenuator, a Glan-Taylor linear polarizer, and a specially designed 4-prism beam expander for achieving the apodization by the tunable Gaussian profile together with the needed beam expansion. During its characterization rather precise adjusting of the incident light beam had been realized. The Fourier-processing part of this spatial arm embraces three key components. The first of them is the above-mentioned rutile AO cell with active optical aperture 60×2 mm^2. The second one is a fragment of the 3-inch achromatic doublet lens

(Edmund Optics) with the focal length of about 85 cm, while the third component represents one of the rows of at least a 3-row multi-pixel CCD-matrix whose pixel has not more than 4.7 μm in width. The performed characterization demonstrates that each individual optical beam can shape spots whose main lobe lights usually about two pixels in the corresponding row of CCD-matrix providing optimal resolution from viewpoint of the sampling theorem. This general optical scheme represents in the main the high-frequency spatial arm for a potential AO spectrometer depicted in Fig. 1.

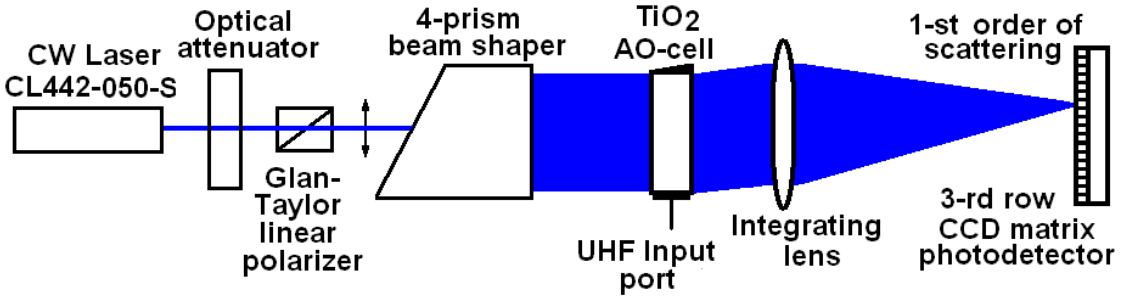

Fig. 10. The high-frequency spatial arm for a potential multi-arm spectrometer with rutile-based AO cell.

The above-mentioned TiO_2-based AO cell with an active optical aperture of 60 × 2 mm^2 was tested within this arrangement as the scheme of experimental set-up. To minimize the optical absorption in this material the blue light (the wavelength is 442 nm, the refractive index for the incident light is $n_E \approx 2.2853$) with linear polarization state of the incident light had been chosen. The anomalous process of light scattering by pure shear mode $S[110][1\bar{1}0]$ with the acoustic wave velocity $V \approx 3.3 \times 10^5$ cm/s had been selected. The performed experiments included two different parts. The first part consisted in estimating the AO frequency bandwidth in the regime of a non-collinear anomalous Bragg light scattering into the first order through observation of the frequency band-shape peculiar to that 60-mm aperture TiO_2 crystalline AO cell. The other one had been directed to determining the frequency resolution of that AO cell via measurements of the distributions inherent in the resolvable spot profiles in a pattern appearing in a focus of the integrating lens for light scattered by the same TiO_2-based AO cell.

Within these experiments, our rutile-based AO cell was illuminated by the single-frequency light beam expanded and polarized linearly in a plane of light scattering, which includes the acoustic beam inside the rutile-based AO cell. Such a state of polarization gave maximal transmission and desirable Gaussian apodization of the prism beam expander because the plane of optical beam expansion was coinciding with the plane of light polarization. Moreover, this polarization state provided the highest efficiency of light scattering within the chosen orientation of a crystal. Exactly the Bragg regime of AO interaction was provided by accurately adjusted angle of light incidence on undoubtedly thick dynamic acoustic grating. The last condition had been satisfied in connection with the above-described condition for the Klein-Cook parameter $Q \approx 5.35 \times 10^2 >> 1$ even in the case of he minimal acoustic frequency f_{min} = 1735 MHz within the bandwidth of AO cell under analysis with the interaction length L = 0.2 cm at λ = 442 nm.

5. EXPERIMENTAL DATA

5.1. General Estimations and Band-Width

Theoretically, the efficiency of a Bragg AO cell at given exciting acoustic wave power density P can be estimated as $I_0 = \sin^2 (\sigma L)$, where $\sigma = (\pi / \lambda)\sqrt{P M_2 / 2}$ [9]. Let us put that the efficiency of AO cell does not exceed 10%, i.e. $I_0 = 0.1$, with $L = 0.2$ cm at $\lambda = 442$ nm. In similar low-efficiency regime, specific for AO processing of radio-wave signals, the effect of a two-phonon light scattering can be omitted [7]. Thus one arrives at $\sigma = \arcsin (I_0^{1/2}) / L \approx 1.60875$ cm $^{-1}$, and $P = 2 I_0 \lambda^2 / (\pi^2 L^2 M_2) \approx 10.58 \cdot 10^7$ g/s^3 $\approx$ 0.106 W/mm^2.

The rutile-based AO cell was prepared to be governed by the radio-wave signals whose best acoustic performances were expected at the central frequency $f_C \approx 2.0$ GHz. A set of electronic equipment for both generating and registering the corresponding electric UHF radio-wave signals had been exploited. The oscilloscope traces of the frequency band-shapes had been recorded by a wide-aperture silicon photo-detector, placed in the integrating lens focal plane. These traces were detected via exploiting the UHF radio-wave sweep-generator simulating the input radio-signal from real astrophysical antenna and the following frequency heterodynes of a radio-telescope.

The frequency of the sweeping signal lied in the range of 1.7 – 2.3 GHz and had been applied to the UHF electronic port of AO cell using the UHF amplifier HD30354 (0.5 – 2.5 GHz, 15 W) and the corresponding impedance-matching electronic circuits. The electronic scheme for optimal connection of the sweep-generator with that port of the AO cell's, i.e. in fact with the ZnO-transducer. We used a two-section wide-band impedance-matching circuit of the lumped electronic components accompanied by a two-cascade resistance step-down transformer assembled out of micro-coaxial cables. These electronic circuits were used to make as wide and uniform as possible the frequency band-shape even at the coast of decreasing the efficiency of the AO cell in part. The single-frequency slow-shear mode with the acoustic power density up to 0.12 W/mm^2 was generated at the swept carrier frequency during the experiments. The efficiency of AO interaction with the pure slow-shear acoustic mode was limited by about 10% to keep the linearity of potential analysis.

The design of this cell, operating in the regime of the one-phonon non-collinear anomalous AO interaction is traditional, which is depicted in Fig. 10. We had exploited the ZnO film oriented along the Y-axes with the coupling factor about of 0.31 and the acoustic impedance 16.4 g/(cm^2 s). Due to the frequency constant 1.44 GHz × μm, this orientation gives the thicker film, more adequate to the expected high-level signals, and provides better acoustical matching with the chosen cut of rutile, whose acoustic impedance is ~ 14.0 g/(cm^2 s). It generated the slow-shear mode acoustic beam with the cross section of about 4 mm^2 at the length $L \approx 0.2$ cm of AO interaction. Additionally, one has to take into account the losses needed for converting the electronic signal into an acoustic one, which are in practice close to 2 – 3 dB. Usually, we have to restrict ourselves to a maximum level $P_{max} \leq 0.5$ W/mm^2 of acoustic power density.

Figure 11 illustrates the normalized plot of the detected frequency band-shape exhibited by the wide-aperture rutile-based AO cell under investigation. Full width of the measured band-shape at a 0.405 level of a maximum can be estimated by the value $\Delta f_M \approx 520$ MHz, see Fig. 11.

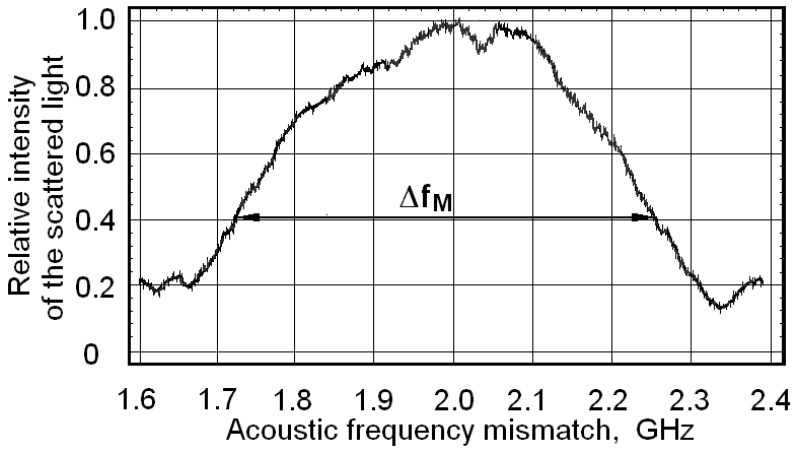

Fig. 11. Experimentally obtained frequency band-shape of a 60-mm aperture rutile AO cell with $\Delta f_M \approx 520$ MHz at a 0.405 level of a maximum .

5.2. Frequency Resolution

Estimating the frequency resolution peculiar to the rutile-based AO cell within the frames of the above-described experimental set-up, including the multi-pixel CCD-array (Toshiba) with 4.7 μm per pixels had been performed at the wavelength 442 nm as well. Two types of measurements had been carried out with a loaded AO cell, i.e. with radio-wave signal applied at the UHF electronic port of that rutile-based AO cell. The first type of measurements had been performed at the central acoustic frequency 2.0 MHz with total acoustic wave attenuation $\widetilde{B} = \Gamma D f_C^2 \approx 8.1$ dB / aperture under action of close to a rectangular, with non-uniformity not more than 10% for the incident lighting. Figure 12 depicts the normalized light intensity profile with the spot size about 7.77 microns and the side lobe level of about 5.1% (about −13 dB) in the focal plane. Our experimental results had been obtained using the achromatic integrating lens (Edmund Optics) with F = 85 cm at the light wavelength 442 nm, so that theoretically $d_T = \lambda F/D \approx 6.26$ μm with D = 60 mm. Together with this, plot in Fig. 12 exhibits $d_M \approx 7.77$ μm due to $\zeta_M \approx 1.241$ and $D_M \approx 48.35$ mm. Factor ζ_M describes the combined effect of imperfectness from AO cell and optical lens. The last data show that almost 19.4% of the active optical aperture inherent in the taken rutile-based crystalline AO cell is lost due to imperfectness of both the lens and the AO cell's crystalline material. Then, instead of theoretical limit for the frequency resolution $\delta f_T = V/D \approx 55.0$ kHz, one yields the measured value $\delta f_M = V / D_M \approx 68.25$ kHz. Thus the experimentally obtained number of resolvable spots can be estimated as $N_M = \Delta f_M / \delta f_M \approx 7620$. Finally, the expected lighted area length in focal plane of the integrating lens can be considered as $L_{CE} = d_M \cdot N_M \approx 59.3$ mm.

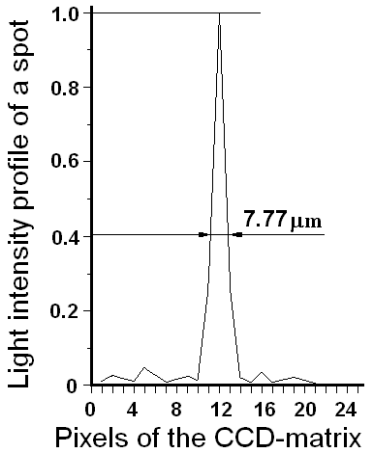

Fig. 12. Light intensity profiles of an individual resolvable spot for the 6-cm aperture rutile-based crystalline AO cell with the applied input UHF radio-wave signal at $f_C \approx 2.0$ GHz.

The second type of measurements had been carried out using Gaussian apodization of the incident light distribution to demonstrate an opportunity of suppressing side lobes and increasing potential dynamic range of data processing within the third spatial optical arm of a prototype under design. In so doing, an almost Gaussian apodization had been shaped exploiting the above-described 4-prism beam expander due to rotating each prism individually and adjusting rather large angles of light incidence as accurate as possible. The light distribution for the case $\beta \approx 6$ (where $I_{in} \approx \exp (2 \beta y^2)$ with $y = x / D$, x is the physical coordinate) is presented in Fig. 13.

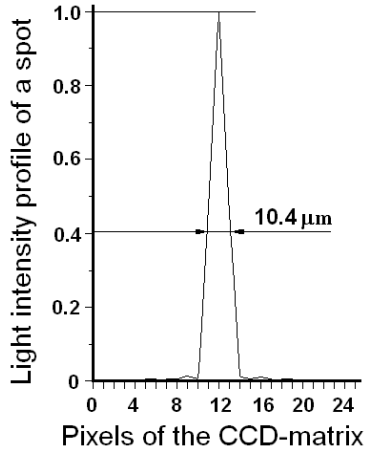

Fig. 13. Light intensity profiles of a resolvable spot for the rutile-based crystalline AO cell with the applied input radio-wave signal at $f_C \approx 2.0$ GHz with Gaussian apodization of the incident light distribution; $\beta \approx 6$.

In this case, the acoustic carrier frequency was again about $f_C \approx 2.0$ GHz with to tal acoustic wave attenuation close to $\tilde{B} \approx 8.1$ dB / aperture. Figure 13 shows the normalized light intensity profile with the spot size about of 10.4 microns with significantly suppressed side lobes, which look as a noise trace at the bottom of this plot. It depicts suppressing the side-lobes significantly. Figure 13 illustrates achieving experimentally the dynamic range approximately 20 dB or even more in the presence of not exactly Gaussian input light profile together with imperfectness of the optical components.

6. CONCLUSIONS

In this paper, we have presented principally new rutile-based AO cell, which is able to provide the development of a wide-band spectrum analysis of astrophysical UHF radio-wave signals. For the first time, we have applied recently developed approach [9] with the tilt angle to a one-phonon non-collinear anomalous AO interaction. In contrast to the earlier cases, now one can exploit the regime with the fixed optical wavelength for processing signals with various acoustic frequencies in linear regime simultaneously.

This unique cell includes both physical and technical novelties. The physical one is represented by the application of recently revealed by us AO degree of freedom to a one-phonon non-collinear anomalous AO interaction. The second novelty consists in an opportunity to regulate the acoustic frequency of that phenomenon and to optimize the frequency performances of operation. We have chosen the rutile crystal as a material that combines a moderate acoustic velocity and relatively low acoustic attenuation allowing operation at UHF of acoustic waves. By the way the optimized optical wavelength λ = 442 nm improves the frequency bandwidth inherent in the rutile AO cell under consideration had been exploited as well.

The taken λ = 442 nm combines the convenience of operating in the visible range with an accessible transparency of this material with blue light. It has been demonstrated experimentally that the rutile-based AO cell of 6 cm aperture is practically able to manage the UHF radio-wave signals at the central frequency about $f_C \approx 2.0$ GHz within the frequency bandwidth ~ 520 MHz at the frequency resolution about 68.25 KHz providing the number $N \approx 7620$ of resolvable spots or parallel UHF channels for spectrum analysis of radio-waves. Together with this, the potential properties of a UHF rutile AO cell, operating in the anomalous light scattering regime has been estimated theoretically. The progressed characterization has shown a possibility of exploiting such an AO cell directly at the central frequency $f_C \approx 2.0$ GHz within the frequency bandwidth ~ 520 MHz with the needed efficiency. Additionally, practical aspects of realizing the Gaussian apodization in a multi-band AO spectrometer have been experimentally examined as well.

The obtained results mean an additional principal development of previously demonstrated innovative design specific to a multi-band AO spectrometer with a few spatially parallel optical arms for the combined processing of their data flows. Similar schematic arrangement permits the simultaneous exploitation of three or more bands at different resolutions and bandwidths, which makes it a highly versatile instrument in a number of astrophysical scenarios. Finally, one can note that, as it has been indicated in the introductory section, the proposed design of a multi-band spectrometer will allow us the construction of a versatile instrument that can be used in virtually every astronomical context, with the advantage that data in three or even more bands can be obtained at the same time. This not only reduces time overheads associated with instrument changes, but allows us to extract valuable data in at least three distinct wavebands. It becomes achievable due to parallel AO processing, that data flows of all the optical arms are united by the joint CCD matrix on the stage of the combined electronic high-bit-rate data processing. At this point one yields at the really united astrophysical instrument, which

provides comprehensive studies of astronomical objects simultaneously with precise synchronization in various frequency scales**.**

ACKNOWLEDGEMENT

Authors would like to acknowledge Dr. Miguel Chavez Dagostino (INAOE) for deep and extremely constructive discussions.and CONACyT for financial support through grant (CB-256961).

REFERENCES

[1] A. S. Shcherbakov, M. Chavez Dagostino, A. O. Arellanes, and E. Tepichin, "An Advanced Multi-Band Acousto-Optical Radio-Wave Spectrometer with Multi-Channel Frequency Processing for Astrophysical Studies", International Journal of Astronomy and Astrophysics, 6 (4),393-409 (2016).

[2] A. S. Shcherbakov and A. Luna Castellanos. "Developing an advanced prototype of the AO radio-wave spectrometer for studying star formation in the Milky Way.", International Journal of Astronomy and Astrophysics. 4 (1), 128-144 (2014).

[3] I. C. Chang, "Tunable acousto-optic filters: an overview," Opt. Eng. 16 (5), 165455 (1977).

[4] A. S. Shcherbakov, A. O. Arellanes, and E. Bertone, "Advanced collinear LiNbO3 acousto-optical filter for astrophysical spectroscopy in the near ultraviolet: exploring the high spectral resolution," J. Astron. Telesc. Instrum. Syst. 1, 045002 (2015).

[5] L. W. J. Kent, "3 GHz bandwidth rutile Bragg cell," Proc. SPIE 7100, 710027 (2008).

[6] A. S. Shcherbakov and A. O. Arellanes, "Calomel-made crystalline acousto-optical cell designed for an advanced regime of noncollinear two-phonon light scattering," Opt. Eng. 55, 037107 (2016).

[7] V. I. Balakshy, V. N. Parygin, and L. I. Chirkov, Physical Principles of Acousto-Optics (Radio I Svyaz, 1985).

[8] A. P. Goutzoulis and D. R. Pape, Design and fabrication of acousto-optic devices (Marcel Dekker, 1994).

[9] A. S. Shcherbakov and A. O. Arellanes, "Advanced regime of the noncollinear two-phonon acousto-optical interaction governed by elastic waves of finite amplitude and optical spectrum analysis", J. Opt. Soc. Am. B 32 (9), 1930-1940 (2015).

[10] J. R. DeVore, "Refractive Indices of Rutile and Sphalerite," J. Opt. Soc. Am. 41, 416-419 (1951).

[11] M. P. Shaskolskaya, ed., Handbook of Acoustic Crystals (Nauka, 1982).

[12] I. C. Chang, "Acousto-Optic Devices and Applications" in Handbook of Optics Vol. II Devices, Measurements, and Properties, M. Bass Ed., (McGraw-Hill, 1995).

[13] E. I. Gordon, "A Review of Acousto-optical Deflection and Modulation Devices," Appl. Opt. 5, 1629-1639 (1966).

[14] R. W. Damon, W. T. Maloney, D. H. McMahon, in Physical Acoustics Vol. 7, W. P. Mason, R. N. Thurston, Eds. (Academic, New York, 1970).

[15] Yu. I. Sirotin, M. P. Shaskolskaya, Fundamentals of Crystal Physics, (Mir Publishers, Moscow, 1982).

[16] A. Yariv, P. Yeh, Optical Waves in Crystals (Wiley, 1984).